

Article

Failure Mechanism of the Yizhuxiang Collapse under the Joint Effect of Freeze–Thaw and Mining

Shenghua Hu ¹, Yuanjun Hu ², Huiyuan Xu ¹, Dong Ai ¹, Jingjing Yuan ¹, Lei Kou ¹, Wei Huang ^{1,3,*} and Chang Zhou ^{2,4,*}

¹ The Seventh Geological Brigade of Hubei Geological Bureau, Yichang 443000, China

² School of Resources and Geosciences, China University of Mining and Technology, Xuzhou 221116, China

³ Hubei Provincial Key Laboratory of Resources and Ecological Environment Geology, Wuhan 430034, China

⁴ National Coal Mine Water Hazard Prevention Engineering Technology Research Center, Suzhou 234000, China

* Correspondence: huangwei@cug.edu.cn (W.H.); changzhou@cumt.edu.cn (C.Z.)

Featured Application: Authors are encouraged to provide a concise description of the specific application or a potential application of the work. This section is not mandatory.

Abstract: At 10:05 a.m. on 4 February 2022, the perilous rock mass Yizhuxiang in Leizu Town, Yuan'an County, Hubei Province, China collapsed on a large scale. The Yizhuxiang collapse was about 35 m in length, 52 m in height, and 29 m in maximum thickness. The volume of the collapse was $5.32 \times 10^4 \text{ m}^3$. It threatened the transport of the national trunk road, destroyed the branch road and some cement mixing station workshops, and caused serious economic losses. The rock mass exposed in the collapse was dolomite with developed joint fractures. Under the effects of mining and unloading, fractures occurred in the rock mass; the top of the rock mass was bent and deformed towards the free face; and tension cracks were formed on the rear edge. The safety ore pillar directly below the collapsed body was compressed and deformed under the action of gravity, thus accelerating the internal deformation of the rock mass and leading to the formation of multiple dominant joints inside the rock mass. In the winter of 2021, the weather was extreme, with heavy snowfall and low temperatures. Under the effects of freeze–thaw, the strength of the rock mass declined and the tension cracks further expanded so that the rock mass experienced an accelerated deformation and finally collapsed. Causes of the collapse include mining activity beneath the collapsed mass and heightened extreme weather. The cause of the landslide disaster in this area is, however, freeze–thaw, which deserves the attention of scholars and the vigilance of the local government.

Keywords: collapse; engineering mining; freeze–thaw



Citation: Hu, S.; Hu, Y.; Xu, H.; Ai, D.; Yuan, J.; Kou, L.; Huang, W.; Zhou, C. Failure Mechanism of the Yizhuxiang Collapse under the Joint Effect of Freeze–Thaw and Mining. *Appl. Sci.* **2023**, *13*, 3801. <https://doi.org/10.3390/app13063801>

Academic Editors: Arcady Dyskin and Fabrizio Balsamo

Received: 26 October 2022

Revised: 8 March 2023

Accepted: 8 March 2023

Published: 16 March 2023



Copyright: © 2023 by the authors. Licensee MDPI, Basel, Switzerland. This article is an open access article distributed under the terms and conditions of the Creative Commons Attribution (CC BY) license (<https://creativecommons.org/licenses/by/4.0/>).

1. Introduction

Since the beginning of the 21st century, global extreme weather events have occurred frequently, causing a large number of geological disasters [1–7]. In the past decade, more than 5000 geological disasters occurred in China on average every year, resulting in hundreds of casualties and a direct economic loss of a CNY-denominated billion Yuan. Collapse is one of the most common, widespread, and harmful geological hazards [8]. From 2015 to 2021, there were 46,885 geological disasters in China, with collapse disasters accounting for 20% of the total. The deformation and failure in a collapse involve a very complex mechanism controlled by geological structure and lithology. The main inducing causes include landforms, meteorological conditions, earthquakes, and human activities [9–13].

As one of the main causes of inducing collapse, human activities (such as road, railway, and airport construction and mining) can change the stress states, landforms, seepage conditions, and other aspects of geological bodies [14–18]. The impact of mining on geological bodies is particularly serious. Mine mining has a particularly serious impact on

geological bodies, which can easily lead to the increase of tension cracks and even collapse, such as the Lianziya collapse in the Three Gorges reservoir area [19,20], the Jiweishan rock landslide in Chongqing in 2008 [21–24], the Guanling landslide in Guizhou [25,26], the Kaiyang phosphate mine collapse in Guizhou [27], and the Nayongpu Sa collapse in Guizhou [28,29] were all affected by mining at the foot of the slope. The Wulong Jiguanling landslide [30–32] occurred under the influence of mining along the slope. The Yanchihe landslide in Yuan'an, Hubei [33–35], the Zhengxiong landslide in Yunnan [36,37], the Furong mountain collapse in Yibin, Hubei [38], and the collapse of the Honglianchi Iron Mine in Hefeng, Hubei [39] were all caused by mining at the bottom of the collapsed body. Based on the deformation body of Yunlong Mountain in Dafang County, Guizhou Province, Huang Gang analyzed the failure mechanism of rock slopes under goaf conditions by means of bottom friction physical simulation tests, UDEC, and FLAC3D, and obtained the mechanism of gentle mining landslides by using physical simulation tests [40].

In foreign studies, there are also cases of collapse or landslides caused by mining. TuanNQ et al. conducted a study on several rockfalls that occurred at the ChauThoi quarry (an old open-pit mine in Binh Duong Province, Vietnam). In the study, geological surveys were performed to obtain site conditions, focusing on rock fractures. Based on the data, kinematic analysis was performed using DIPS software to identify rock slope failures. The results are then used for rockfall analysis [41]. P. Be'rest et al. performed a retrospective analysis of a case study using empirical and numerical methods using the collapse of Clamart (south of Paris, France) as an example. The cause of the collapse is the lack of bearing capacity of the columns and the sudden rupture of the hard limestone bed where loads accumulate on them until overloading occurs. The weak bed between the two seams also contributes to the general lack of stability in the mine [42]. Chiara Del Ventisette focused on the results of simulation models to better understand the Vaiont collapse, gaining insight into the internal and surface deformation patterns of the sliding rock mass. Plan-view reconstructions of surface model displacements revealed that the rock mass was subdivided into compartments with different relative motions and differential rotations, which played an important role in causing the rapid collapse [43]. Tokgöz N et al. investigated the impact of land use change on the stability of the Agakri landslide in the northern coastal region of Istanbul (Turkey), spanning mining, reclamation, and afforestation. Geological and geophysical surveys were conducted to determine the effect of erosion on the landslide [44]. A landslide event has occurred at the phosphate Kef Essenoun open-pit mine associated with the Jebel Onk mine in northeastern Algeria. MezamMC et al. performed a retrospective analysis of this phenomenon and derived the morphological, geological, hydrogeological, and geotechnical characteristics of the deposit, as well as the main causes that may have been the triggers for this landslide [45].

Under the effect of the freeze–thaw cycle, the rock mass structure deteriorates, and the strength decreases rapidly, especially in the rock mass-containing joints [46]. The joints in the rock provide dominant planes of deformation. However, there are few studies of the mechanism of deformation and failure in a collapse under the joint effect of freeze–thaw and mining.

Located in Hubei Province, China, Yizhuxiang was a perilous rock mass formed after the mining of the Liushangou phosphate mine. With a volume of $5.32 \times 10^4 \text{ m}^3$, the perilous rock mass collapsed at 10:05 a.m. on 4 February 2022, destroying the plant and the road at the slope toe. Based on field investigation and field monitoring, this paper analyzes the deformation evolution process in the Yizhuxiang collapse and reveals the deformation and failure mechanism of the Yizhuxiang collapse. The prevention and control of collapses in low-altitude, low-latitude, and warm regions should also attract the attention of scholars and governments, and also provide a certain basis for the prevention and control of collapses caused by freezing and thawing.

2. Geological Conditions of the Yizhuxiang Collapse

2.1. Geological Structure

The rock mass Yizhuxiang was located in Leizu Town, Yuan'an County, Hubei Province, China, and it is about 53 km away from the seat of Yuan'an County (Figure 1). The landform of the studied area was a low and medium-height mountain. The area was developed with a gentle monoclinal structure, and the rock layer dips 6–15° toward 70–120°. The terrain was high in the west and low in the east, with a relative height difference of 801.0 m. The stratum was dominated by Sinian dolomite, and the goaf was located between dolomite and gneiss. In the studied area, there were many cliffs [47], with a gradient of about 30–45°.



Figure 1. Stable geographical location of the rock mass Yizhuxiang.

The perilous rock mass Yizhuxiang was “columnar”, had an elevation of 680–732 m and a vertical height difference of about 200 m from the road surface. The Yizhuxiang collapse had three free faces and steep fractures developed on the rear edge. National road G347 and a temporary mixing station were at the toe of the collapse (Figure 2). The rock mass collapsed as a whole along the master fracture on the rear edge. It was about 35 m in length, 52 m in height, 29 m in maximum thickness, and $5.32 \times 10^4 \text{ m}^3$ in volume. It was a medium rock collapse with a dominant collapse orientation of 170° and controlled by the master joints. The perilous rock mass was Sinian Dengying Formation (Z2dn) dolomite and dips 15° toward 95°. The top of the perilous rock mass was demolished by blasting on 3 August 2015.

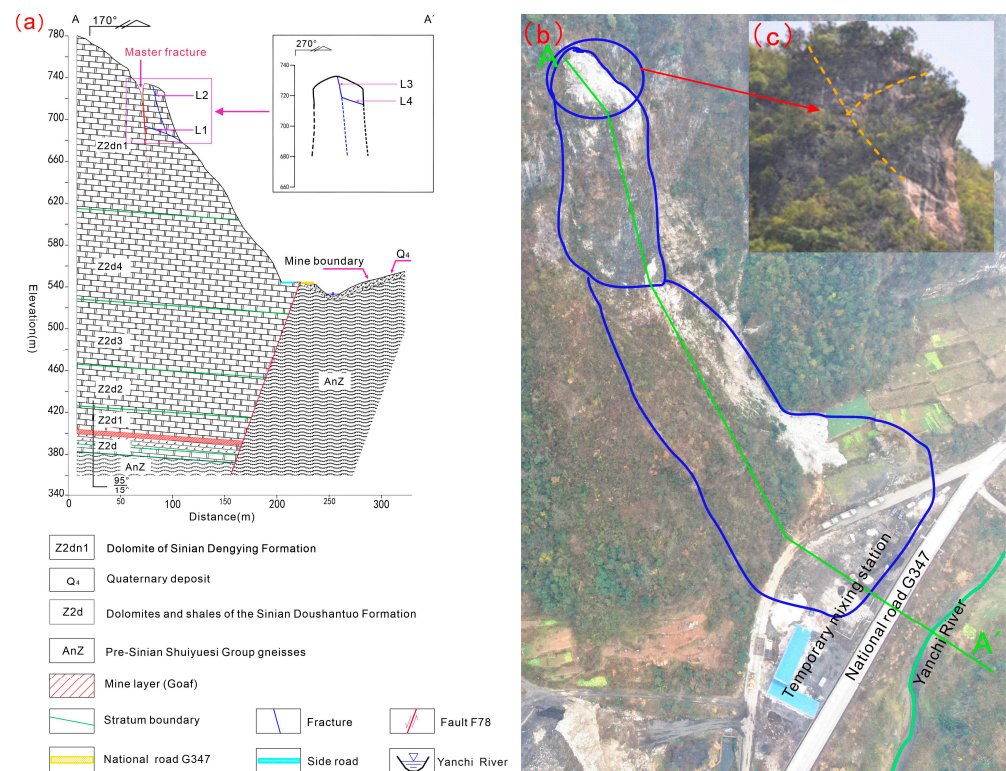


Figure 2. Geological profile of the perilous rock mass Yizhuxiang: (a) Sectional view of Yizhuxiang collapse body; (b) Photos of the landform before the collapse of the Yizhuxiang collapse; (c) Partial photos of the dangerous rocks at the top of the Yizhuxiang collapse before the blasting.

2.2. Hydrology and Weather

The Yizhuxiang colluvium area has a subtropical monsoon climate with humid air and abundant precipitation. The average temperature was 15.9 °C. The annual maximum and minimum temperatures were 40 °C and −13.5 °C, respectively. The annual average precipitation was 1114.5 mm. It is cold in winter and has a long period of ice and snowfall. The period from December to March of the next year is a period of intermittent freezing. The maximum snow depth was about 300 mm. The land surface temperature in February 2022 was about 5 °C lower than in previous years (Figure 3b). The average temperature from the end of January to the beginning of February fluctuated around 0 °C (Figure 3d). The snow depth was 4.07 times that in 2021 (Figure 3a).

2.3. Characteristics of the Goaf

The mining of underground phosphate ores in the studied area was started in 2013 and stopped in July 2014. The goaf was nonfirmly backfilled with slag muck. The total area of the goaf was about 0.5 km². The safety pillars in the goaf had section dimensions of 1.5 m × 3 m and 2 m × 2 m and had a spacing of about 12.5–15 m. The safety pillars remained under the rock mass Yizhuxiang, with a length and width of 61 m and 52 m, respectively (Figure 4). An investigation in 2015 showed that the rock was relatively fragmented after the pillars were squeezed and collapsed. Structural fractures were relatively developed in the roof, and roof fall occurred. Three floor heaves were found on the floor. They had a height of 0.20–0.5 m and a maximum floor heave of 1.10 m. This showed that the tunnel and the safety pillars were subjected to great stress.

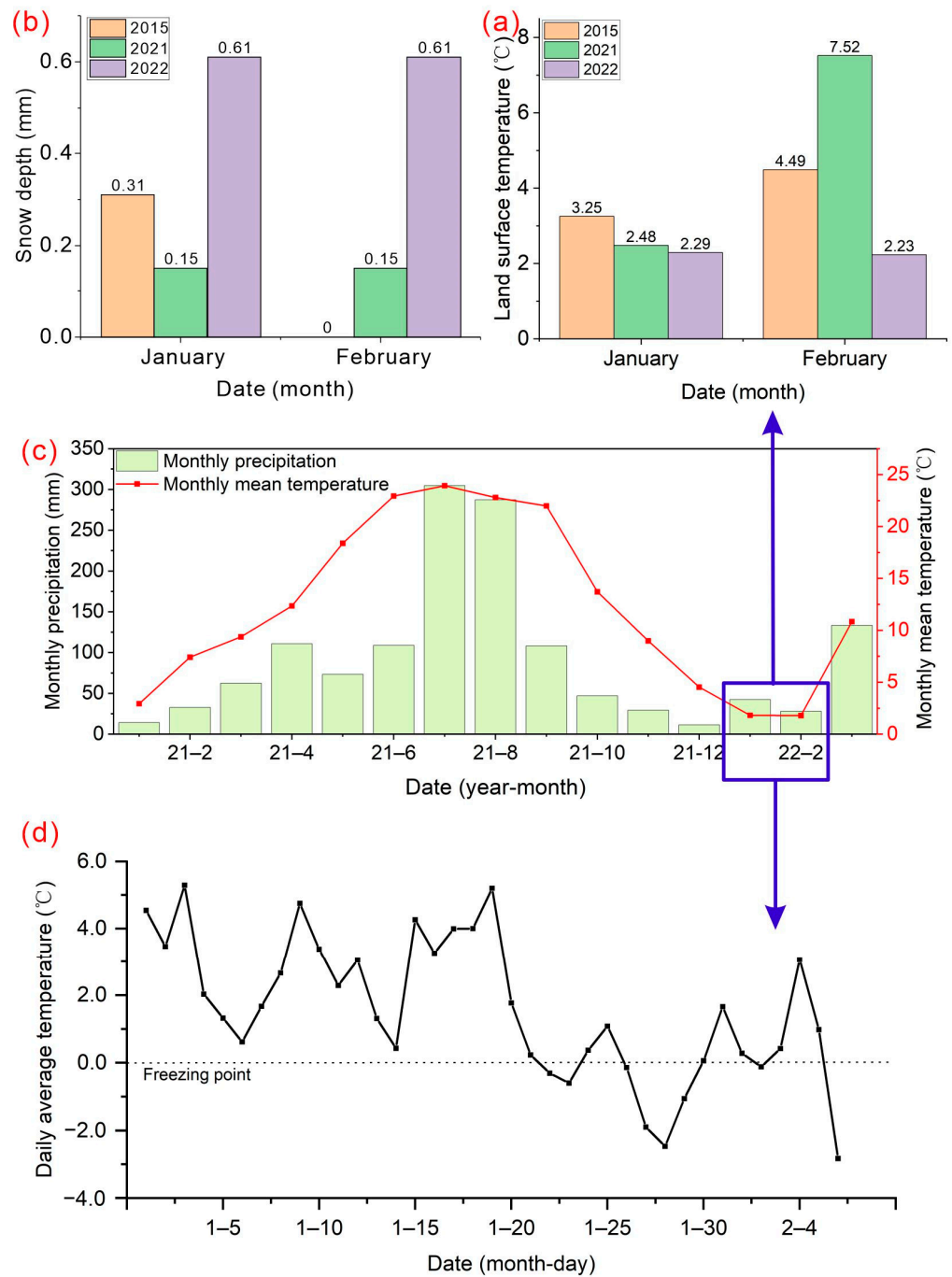


Figure 3. Comparison of the weather conditions in the studied area in 2021 and January and February of 2015, 2021, and 2022: (a) Comparison of snow depth in January and February in the study area; (b) Comparison of surface temperature in January and February in the study area; (c) Climate conditions in the study area from January 2021 to March 2022; (d) Daily air temperature changes before and after the collapse of Yizhuxiang in the study area.

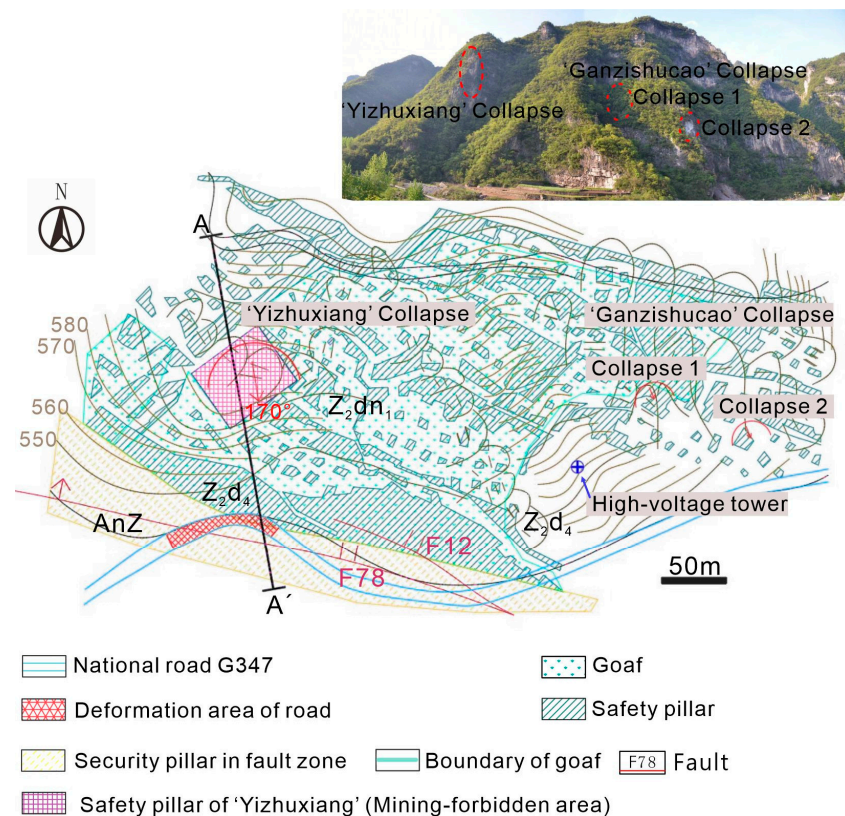


Figure 4. Floor plan of the goaf in the studied area.

3. Deformation and Failure Characteristics of the Collapse

3.1. Deformation Process of the Yizhuxiang Collapse

After the tunnel was closed in July 2014, cracks appeared on the rear edge of the rock mass Yizhuxiang. On 8 July 2014, the perilous rock mass Ganzishucao about 260 m away from the rock mass Yizhuxiang collapsed due to precipitation and other weather causes (Figure 4a). The “collapse 1” of the overall collapse had a size (length \times height \times thickness) of 5 m \times 4 m \times 2.5 m and had a volume of 68 m³. The “collapse 2” of the overall collapse had a size (length \times height \times thickness) of 8 m \times 5 m \times 3 m and had a volume of 120 m³. In February 2015, the road under the rock mass Yizhuxiang cracked. In March 2015, the width of the master fracture of Yizhuxiang increased significantly. According to the fracture width monitoring data, the crack width began to increase gradually with the increase of precipitation after 26 February 2015. The nearby Ganzishucao had fallen rocks. Therefore, the top of the perilous rock mass Yizhuxiang and the top of the perilous rock mass Ganzishucao were removed by blasting at 11:58 a.m. on 3 August 2015 (Figure 2c). However, according to the residents, the fractures on the rear edge of the rock mass widened significantly. New cracks were found on National Road G347 after March 2016. At 10:05 a.m. on 4 February 2022, the rock mass Yizhuxiang collapsed. At the end of the collapse, the colluvium area still frequently experienced falls of small rocks and “white smoke” caused by rock mass compression.

3.2. Deformation and Failure Characteristics of the Yizhuxiang Collapse

A field investigation was carried out after the deformation of the perilous rock mass significantly increased in 2015. The investigation found that the base surface was obviously split (Figure 5a), and had several traces of spalling of small-sized blocks with a diameter of 5–37 cm. In addition, traces of fracturing opening (Figure 5b) were developed on the structural plane of the master fracture on the west side of the base and showed twist compression towards the southeast. The rock mass was flaky. This showed that the

structural plane of the master fracture on the rear wall of the rock mass was in the stage of development and extension from top to toe, and from west to east, gradually cutting the rock mass from the base into an independent block.

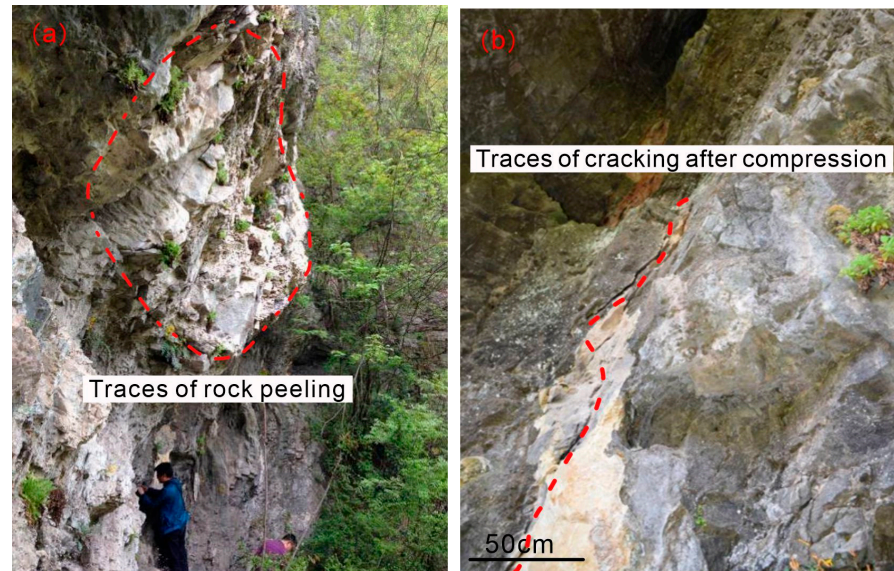


Figure 5. Deformation of the rock base on the east side of the rock mass Yizhuxiang: (a) Rock spalling on the base surface on the east side of the collapse body; (b) Opening traces of fracturing at the base on the east side of the collapse.

The rock mass was developed with joint fractures, including five dominant fractures in total: master fracture, L1, L2, L3, and L4 (Figure 2, Figure 6). The master fracture on the rear edge dips 83° toward 190° . The fracture surface was rough and locally filled with broken stones. The master fracture controlled the stability of the whole perilous rock mass. Figure 7b shows the changes of master fracture at the posterior edge of the dangerous rock mass and road cracks under the condition of rainfall. From 2 January to 8 February 2015, the width of the master fracture was basically unchanged. However, after the precipitation on February 26, the fracture width increased significantly and gradually increased at a rate of 0.13 mm/day. After 11 March, the displacement rate further increased to 0.37 mm/day. The cumulative displacement reached 25 mm on 10 April, and then gradually became stable. The crack on the road at the slope toe showed the same change trend. From 10 February to 27 March, the cumulative width of the crack reached 40 mm. On 15 April, the cumulative width reached 49 mm and then became stable. On 27 April, the cumulative displacement experienced a stepwise increase. The precipitation in the studied area had obvious characteristics from the end of February to the beginning of April. The daily precipitation increased, and the duration of precipitation increased. The precipitation on 17 March reached 33.528 mm, more than three times that on 10 February, and 15 times that on 29 January. Every day in the 14 days from 26 March to 8 April was a day of precipitation. After that, the precipitation frequency decreased significantly, however, the single-day precipitation was heavy. In 2015 (Figure 3a,b), the average snow thickness depth was 0.31 mm in January and there was basically no snowfall, and the land surface temperature was relatively high after February. The snow depths in January and February 2022 were much higher than those in 2015 and 2021, and the surface temperature in January and February 2022 was lower than those in previous years. Compared with January 2021, January 2022 had a similar temperature and higher precipitation (Figure 3c). Compared with February 2021, February 2022 had similar precipitation and a lower temperature. Therefore, the changes in the cracks were particularly obvious from the end of February to the beginning of April 2015, and the changing trend was similar to that of precipitation.

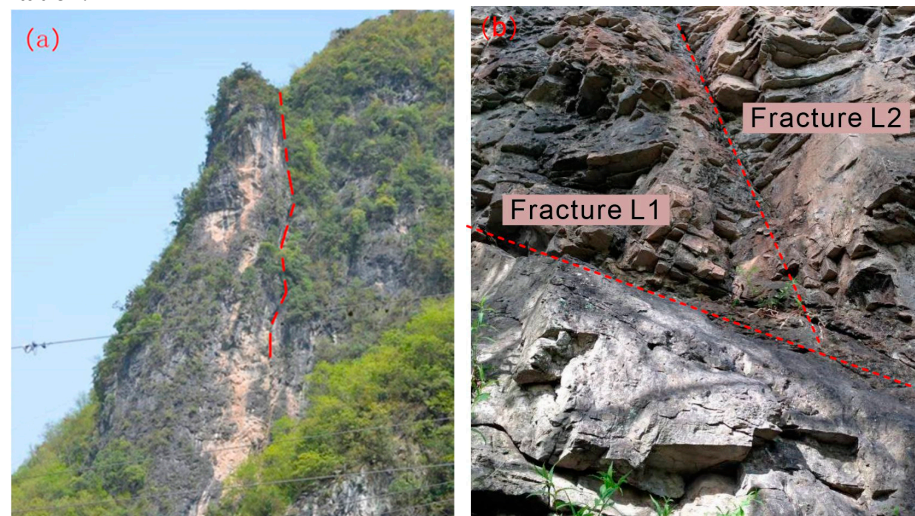


Figure 6. (a) Master fracture (before blasting) (b) Fracture L1 and Fracture L2 intersected.

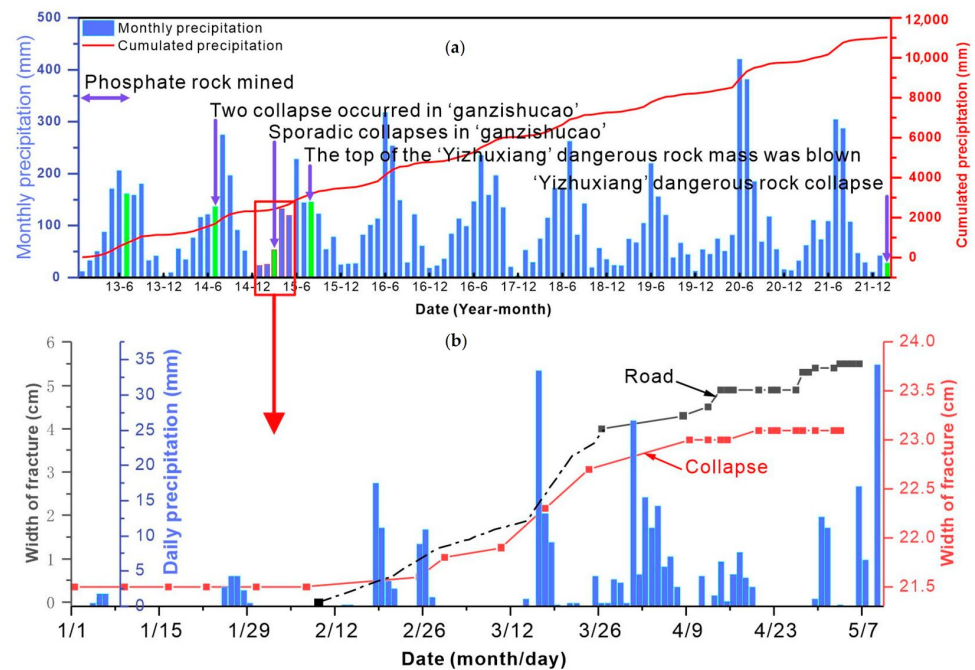


Figure 7. (a) Major events during the deformation process of the collapsed body; (b) Changes in master fracture [48] and road cracks under rainfall.

The other four dominant fractures—L1: dips 33° toward 180° , about 18 m in length, the fracture surface is slightly open and straight, extending toward the rear wall of the dangerous rock mass; L2: dips 76° toward 175° , about 30 m in length, 1–5 cm in average crack width and 20 cm in maximum width; L1 and L2 intersected (Figures 2 and 6b); L3: dips 82° toward 285° , about 30 m in length, about 5–30 cm in fracture width; L3 was located on the back (north side) of the rock mass and developed from top to toe, with a rough crack surface. It was filled with broken stones and relatively fragmented stones at the bottom of the fracture; L4: dips 35° toward 210° , about 4 m in length and about 5–10 cm in width; L3 and L4 intersected. The rock mass at two fracture openings was obviously weathered. The surface of the rock mass on the rear (north side) was obviously split. There were signs of collapse and block falling near both the west and the east “base”, and “cavities” had been formed locally. The above content is the description of the morphology of the four nonmain control fractures by the surveyors in August 2015. According to

observation and research, it is found that with the passage of time, the length and width of cracks have a strong positive correlation with precipitation.

Figure 8 shows that the rocks in the collapse mainly rolled down along the slope, with some fallen rocks scattered on the slope, including two large solitary stones standing still on the slope and with dimensions of (length \times width \times height) $3\text{ m} \times 4\text{ m} \times 5\text{ m}$ and $1.5\text{ m} \times 1.5\text{ m} \times 3\text{ m}$. The fallen rocks had a total volume of about $1 \times 10^4\text{ m}^3$. Some of them were on the right side of the main colluvium area of the fallen rocks (major colluvium area), with a maximum block size of $25\text{ m} \times 4\text{ m} \times 4\text{ m}$, damaging farmland, the road, and the factory plant. The other fallen rocks were located in front of the rock mass, causing partial damage to the temporary cement mixing station and the road. According to the field investigation, a large “wedge-shaped” fallen rock remaining in the colluvium area had a volume of about 6000 m^3 . The rear fractures running from top to bottom can be observed on both the east and west sides of the residual perilous rock, with a width of 5–20 cm. The residual rock mass in other areas had a volume of about 500 m^3 , and some residual perilous rocks were unstable. The solitary stones on the slope seriously affected the safe operation of National Road G347 and the temporary mixing station below them.



Figure 8. (a) Fractures ran through the rear edge on the west side of the residual perilous rock; (b) Fractures ran through the rear edge on the east side of the residual perilous rock; (c) Solitary stones on the slope; (d) Full view after the collapse of the perilous rock mass; (e) Colluvium area of fallen rocks at the slope toe.

4. Deformation and Failure Mechanism

4.1. Analysis of Inducing Causes

Geological impact: the stratigraphic dip of the studied area Yizhuxiang was 95° . The slope in the perilous rock area was a tangential slope, and the rock attitude was relatively gentle (15°). The upper part of the studied area was Dengying Formation dolomite, which has a strong weathering resistance and tends to form large and steep cliffs with free faces. The rock mass was relatively fragmented due to the impact of fracture cutting. The lower part is Doushantuo Formation siliceous dolomite, shale, and phosphate rock bed, which has weak weathering resistance and relatively low strength and tends to form a gentle slope (Figure 2). Under this rock stratum combination, soft layers such as shale at the bottom are prone to plastic deformation under the gravity of the overlying rock mass and lead to the cracking of the hard rock stratum prone to brittle fracture in the upper part. The structure of hard strata in the upper part and soft strata in the lower part created the geological environment and material conditions for the formation of collapse [49,50].

In 2015, the widths of the cracks on the rear edge of the perilous rock mass and the road cracks were positively related to the daily precipitation (Figure 7b). That is, the infiltration of precipitation increased the water content of the rock mass, thereby softening the structural plane of the rock mass, changing the mechanical state of the structural plane, and decreasing the antioverturning moment, so that the fractures on the rear edge of the rock mass became gradually connected [51–54]. Similarly, the fracture water pressure will cause additional deformation of the rock block, resulting in an increase in the opening of the fracture and an increase in the permeability coefficient. The shearing strength of dolomite decreased rapidly with the increase in water content so that the plastic deformation increased and the ductility after failure was significantly enhanced [55]. In 2022, extreme weather events occurred, with the snowfall much higher than those in previous years and the temperature significantly lower than those in previous years. As a result, the collapse occurred before the rainy season, indicating that the rock mass was continuously subjected to repeated freezing and thawing. In the process of freeze–thaw cycles, the damage of the water–ice phase change on the rock mass was gradually accumulated, specifically with the temperature change, the water-filled structural plane repeatedly froze and thawed, resulting in progressive rock mass damage caused by gradual splitting, and the elastic modulus, hardness, and fragmentation of dolomite were negatively related to the number of freeze–thaw cycles [56–60]. Especially for rock masses with fissures, the frost-heaving force caused by the freezing process of the fissure water is an important reason for the deterioration of the rock mass structure [61,62]. The lower the freezing temperature, the earlier the frost heave force will appear. The closer it gets to the freezing point [63]. Under the action of multiple freeze–thaw cycles, during the process of continuous accumulation, explosion and release of frost-heave force, a single fracture surface develops into multiple fracture surfaces, and the accumulated damage of cracks leads to further expansion and penetration of cracks [61]. The aforesaid causes ultimately led to a collapse.

Mining was one of the main causes causing the collapse. During the mining process, the rock mass is under the action of unloading, which is mainly subjected to tension damage and shear damage [64], which induces cracks in the rock mass, and the security pillars left after mining provide sufficient support for the top rock mass. After mining operations ended, the pillars began to spall and collapse [65]. Under the action effect of pressure, the safety pillars were subjected to stress concentration at the corners and then broke (Figure 9a) [66]. When the pressure increased, the cracks inside the rock expanded, and new cracks were generated. The direction of the cracks was mainly vertical (Figure 9b). When the goaf continued to expand, the force shared by each pillar increased correspondingly, so that the internal cracks continued to expand, new shear cracks were generated, and the rocks on the pillar surface continued to spall (Figure 9c). Finally, when the cracks expanded to a certain extent, the strength of the pillar-supported rock mass was greatly reduced. When the force on the rock mass was greater than the strength of the rock mass, the pillars failed (Figure 9d). The main forms of pillar failure were peeling and necking of the pillar

surfaces. With the deformation of the pillars, the fractures in the upper rock mass gradually expanded [67].

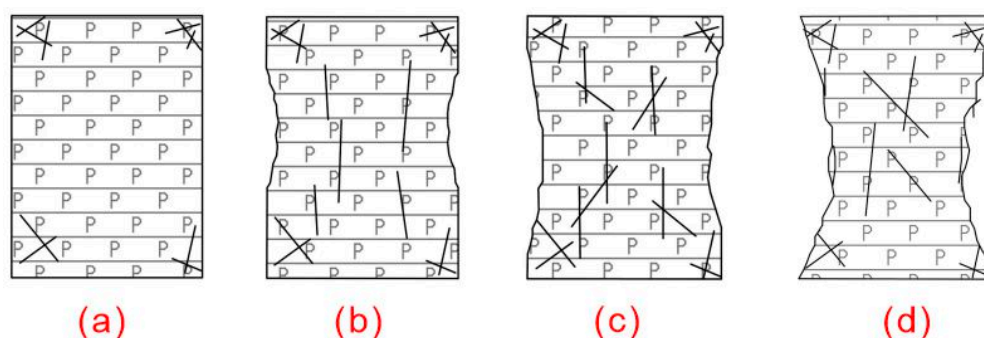


Figure 9. Pillar cracking and failure evolution process: (a) Pillar corner stress concentration, resulting in peeling; (b) Pillar surface peeling, internal pressure crack; (c) Pillar surface continued to peel off, producing oblique shear stripes; (d) Pillars failed, leaving little residual strength.

Below the dangerous rock is a temporary mixing plant and National Road G347. Large vehicles are busy on the road, and the rocky slope is subjected to traffic cycle vibration caused by long-term cyclic loads of vehicles. In addition, the blasting vibration of long-term excavation and mining and the deep-hole blasting and demolition of the rock at the top of “Yizhuxiang” caused fatigue damage to the rock mass, and the cumulative effect slowly caused the structural surface of the rock mass to loosen and reduce the strength of the rock mass. Therefore, the interference of the outside world with the rock is also one of the reasons for the connection of cracks inside the dangerous rock and the collapse of the dangerous rock mass [68,69].

4.2. Collapse Evolution Process

The collapse deformation process can be divided into four stages by the deformation and failure characteristics.

Fracture formation stage: during underground mining, cracks were formed in the rock mass under the joint effect of vibration loading and unloading. In addition, the continuous deformation of the pillars caused cracks in the rock mass. (Figure 10a).

Rear edge fracture formation stage: As dolomite was eroded and softened by precipitation, the existing internal fractures gradually developed and became connected. In addition, mining promoted the gradual expansion of the fractures to form dominant fractures. The top of the rock mass was bent and toppled under the action of gravity, and the fractures on the rear edge of the rock mass gradually expanded to the deeper part (Figure 10b).

Collapse formation stage: due to the deformation of safety pillars and the blasting of the perilous rock, the internal cracks became connected, and the rock mass was bent and toppled, and the master fractures on the rear edge gradually expanded. The precipitation infiltrated along the fractures, generating hydrostatic pressure, reducing the mechanical strength between the rock mass and the structural plane, increasing the downward and outward movement force of the unstable rock mass, and finally leading to collapse (Figure 10c).

Fracture penetration stage: Compared with previous years, the weather in the winter of 2021 changed greatly, with an increased snowfall and a low temperature, leading to more significant freezing and thawing, which caused the destruction of the rock mass structure, the gradual penetration and expansion of the fractures, and the accelerated deformation of the rock mass, and finally resulted in the complete penetration of the fractures on the rear edge of Yizhuxiang and the failure of the rock mass (Figure 10d).

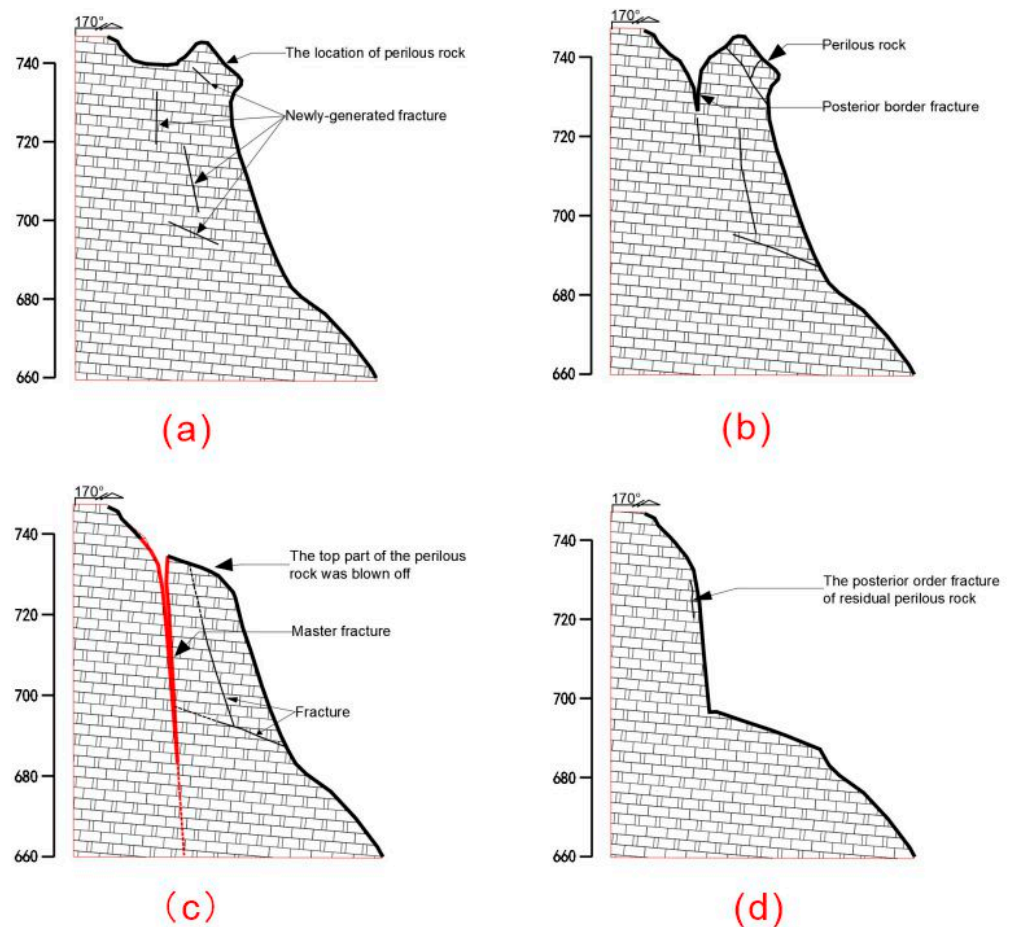


Figure 10. Evolution process of Yizhuxiang collapse; (a) Fracture formation stage; (b) Rear edge fracture formation stage; (c) Collapse formation stage; (d) Fracture penetration stage.

5. Conclusions

Under the effects of mining and precipitation, the rock mass Yizhuxiang underwent continuous deformation in 2015, and the top rock mass was bent and toppled, and master fractures and four dominant joints were formed in the rock mass. In 2022, the extremely cold weather led to the overall failure of the rock mass Yizhuxiang, which damaged the farmland, the temporary cement mixing station, and the road at the slope toe. The Yizhuxiang collapse had multiple causes, including mining, precipitation, and geological conditions.

- (1) Geological structure: the rock mass Yizhuxiang had three free faces. The stratum was dominated by brittle dolomite, hard at the top and soft at the bottom. The studied area experienced frequent and considerable precipitation and strong weathering. Water flowing into the rock fractures increased the static and dynamic water pressure on the rock mass, and increased the lateral pressure on the free faces of the rock mass, which was not conducive to the stability of the rock mass;
- (2) External disturbance: The mining of phosphate ores at the bottom of the studied area was stopped in July 2014, and the safety pillars remaining at the lower part of the rock mass continued to be deformed, accelerating the deformation of the upper rock mass and the expansion of fractures. Continuous precipitation increased the water content of the stratum, and the joint action of seepage softening and pore pressure caused the cracks and joints to go deeper and become wider, and gradually penetrate downward. In 2015, the deep-hole blasting of the perilous top of the rock mass Yizhuxiang also caused fatigue damage to the rock mass. The cumulative effect gradually caused the looseness of the structural plane of the rock mass and reduced the strength of the rock mass;

- (3) Freeze-thaw effect: from January to February 2022, Yuan'an County had a low average temperature and a snowfall much deeper than those in previous years. The effect of freeze–thaw became the main factor finally inducing the collapse. The collapse caused by freezing and thawing is caused by the frost-heaving force generated by water. When dealing with a collapse disaster caused by freezing and thawing, the salinity of surface water can be changed to reduce the freezing point of water.

Collapses caused by freezing and thawing can also occur in areas with low latitudes, low altitudes, and warm and humid climates, which has played a role in improving the prevention and control of collapses in low latitudes and low altitudes.

Author Contributions: Conceptualization, W.H. and C.Z.; Methodology, S.H.; Validation, W.H.; Investigation, H.X., D.A. and L.K.; Resources, J.Y.; Data curation, H.X.; Writing—review & editing, S.H., Y.H. and C.Z.; Visualization, W.H.; Supervision, S.H.; Project administration, S.H. and W.H.; Funding acquisition, C.Z. All authors have read and agreed to the published version of the manuscript.

Funding: This work was supported by the following 5 funds, programs, projects: Key R & D Program of Xinjiang Uygur Autonomous Region (2021B03004-3), The Natural Science Foundation of Jiangsu Province (BK20221126), National Natural Science Foundation of China (42207169), China Postdoctoral Science Foundation (2022M710177), The Seventh Geological Brigade of Hubei Geological Bureau science and technology project (DQKJ2022-1, DQKJ2022-2).

Institutional Review Board Statement: Not applicable.

Informed Consent Statement: Not applicable.

Data Availability Statement: The data presented in this study are available on request from the lead author.

Conflicts of Interest: The authors declare that they have no known competing financial interest or personal relationship that could have appeared to influence the work reported in this paper.

References

- Zhu, Z.; Huang, N.; Kuang, Y.; Ouyang, T.; Deng, Y.; Zheng, J.; Zhang, J.; Zheng, T.; Wu, Y.; Qiu, S. Coping with global climate change and frequent geological disasters. In Proceedings of the 4th Guangdong-Hong Kong-Macao Symposium on Sustainable Development 2008, Guangzhou, China, Macau, China; Hong Kong, China. 25–28 September 2008; pp. 350–353.
- Tippett, M.K. Extreme weather and climate. *NPJ Clim. Atmos. Sci.* **2018**, *1*, 45. [[CrossRef](#)]
- Helmer, M.; Hillhorst, D. Natural disasters and climate change. *Disasters* **2006**, *30*, 1–4. [[CrossRef](#)] [[PubMed](#)]
- Huang, Y.; Cheng, H. The impact of climate change on coastal geological disasters in southeastern China. *Nat. Hazards* **2013**, *65*, 377–390. [[CrossRef](#)]
- Huggel, C.; Salzmann, N.; Allen, S. High-mountain slope failures and recent and future warm extreme events. In *Climate Forcing of Geological Hazards*; McGuire, B., Maslin, M., Eds.; Wiley-Blackwell: Chichester, UK, 2013; pp. 195–222.
- Liggins, F.; Betts, R.A.; McGuire, B. Projected future climate changes in the context of geological and geomorphological hazards. *Philos. Trans. R. Soc. A* **2010**, *368*, 2346–2347. [[CrossRef](#)]
- Qu, X.; Li, Y.; Yang, X.; Fang, H.; Yin, C. The general characteristics and situation analysis of geo-hazards in China. *Chin. J. Geol. Hazard Control* **2016**, *27*, 109–113.
- Hu, H. Preliminary investigation on the classification of collapse. *Railw. J.* **1985**, *7*, 90–100.
- Wang, F.; Wang, S.; Zhou, Y.; Wang, L.; Yan, F.; Li, W.; Liu, X. High resolution remote sensing monitoring and assessment of secondary geological disasters triggered by the Lushan earthquake. *Spectrosc. Spectr. Anal.* **2016**, *36*, 181–185.
- Zhi, K.; Pan, J. Cause analysis and control measures of collapse geological disaster. *China Met. Notif.* **2022**, *8*, 187–189.
- Tian, S.; Kong, J.; Fan, X.; Ding, M. Before and after the lushan earthquake contrast geohazards in earthquake-stricken areas. *Mt. Res.* **2014**, *32*, 111–116.
- Lü, Y.; Chen, T.; Wang, Z.; Zhao, J.; Zhan, J.; Liu, X. Study on the development characteristics and genetic patterns of collapses in The Taihang mountain Grand Canyon, China. *J. Eng. Geol.* **2022**, *30*, 1304–1315.
- Hu, C. Rock fall evaluation model in mountain highway. *Commun. Stand.* **2007**, *7*, 53–56.
- Zou, P.; Tang, C.; Wang, S. Human activities and induced geological disasters. *Impact Sci. Soc.* **1998**, *1*, 14–19. [[CrossRef](#)]
- Zhang, Y. Disaster characteristics of collapse, landslide and debris flow in China and socialization of disaster reduction. *Disaster Reduct. China* **1996**, *6*, 27–30. [[CrossRef](#)]
- Qian, L.; Zang, S. Differentiation Rule and Driving Mechanisms of Collapse Disasters in Changbai County. *Sustainability* **2022**, *14*, 2074. [[CrossRef](#)]

17. Qian, L. Present situation and prevention measures of geological disasters induced by human activities in Huadian City, Jilin Province. *Jilin Geol.* **2014**, *1*, 131–133, 140.
18. Guzzetti, F.; Reichenbach, P.; Ghigi, S. Rockfall Hazard and Risk Assessment Along a Transportation Corridor in the Nera Valley, Central Italy. *Environ. Manag.* **2004**, *34*, 191–208. [[CrossRef](#)] [[PubMed](#)]
19. Keqiang, H.; Guangming, Y.; Xiangran, L. The regional distribution regularity of landslides and their effects on the environments in the Three Gorges Reservoir Region, China. *Environ. Geol.* **2008**, *57*, 1925–1931. [[CrossRef](#)]
20. Le, Q.; Wang, H.; Xue, X.; Gao, Y.; Jin, X.; Zhang, J.; Pan, S. Deformation monitoring and failure mechanism of Wangxia dangerous rock mass in Wushan county. *J. Eng. Geol.* **2011**, *19*, 823–830.
21. Liu, C. Mechanism Analysis on the Jiweishan rockfall disaster happened in Wulong, Chongqing, 5 June 2009. *J. Eng. Geol.* **2010**, *18*, 297–304. (In Chinese)
22. Xu, Q.; Huang, R.; Yin, Y.; Hou, S.; Dong, X.; Fan, X.; Tang, M. The Jiweishan landslide of 5 2009 June in Wulong, Chongqing: Characteristics and failure mechanism. *J. Eng. Geol.* **2009**, *17*, 433–444. (In Chinese)
23. Qiang, X.; Xuanmei, F.; Runqiu, H.; Yueping, Y.; Shengshan, H.; Xiujun, D.; Minggao, T. Landslides volume. A catastrophic rockslide-debris flow in Wulong, Chongqing, China in 2009: Background, characterization, and causes. *Landslides* **2010**, *7*, 75–87.
24. Feng, Z.; Yin, Y.; Li, B.; Zhang, M. Mechanism analysis of apparent dip landslide of Jiweishan in Wulong, Chongqing. *Rock Soil Mech.* **2012**, *33*, 2704–2712. (In Chinese)
25. Jianjiang, Z.; Shengyuan, Y.; Rui, W. Inspiration of “628” major geological disaster in Guanling, Guizhou. *Chin. J. Geol. Hazard Control* **2010**, *21*, 137–139.
26. Yin, Y.; Zhu, J.; Ang, S. Investigation of a high speed and long run-out rockslide-debris flow at Dazhai in Guanling of Guizhou province. *J. Geomech.* **2010**, *18*, 445–454.
27. Zheng, D.; Huang, R.; Huang, G. Mechanism of rockfall with anti-dip and top hard-bottom soft rock by underground mining—A case study of rockfall in Kaiyang phosphorite, Guizhou. *J. Eng. Geol.* **2014**, *22*, 464–473.
28. Liang, F.; Shi, W.; Qian, X.; Yu, X.; Xiong, S. Study on deformation and failure mechanism of gentle anti-dipped slope induced by mining in mountain area: A case study of the Pusa village rock avalanche of Guizhou. *J. Nat. Disasters* **2022**, *31*, 190–200.
29. Zheng, G.; Xu, Q.; Ju, Y.; Li, W.; Zhou, X.; Peng, S. The pusacun rockavalanche on august 28, 2017 in Zhangjiawan Nayongxian, GuiZhou: Characteristics and failure mechanism. *J. Eng. Geol.* **2018**, *26*, 223–240.
30. Wang, G.; Li, B.; Feng, Z.; Xing, A. Simulation of the process of the Jiguanling rock avalanche in Wulong of Chongqing. *Hydrogeol. Eng. Geol.* **2014**, *41*, 101–106.
31. Li, B.; Feng, Z.; Wang, G.; Wang, W. Processes and behaviors of block topple avalanches resulting from carbonate slope failures due to underground mining. *Environ. Earth Sci.* **2016**, *75*, 1–26. [[CrossRef](#)]
32. Kai, H.E.; Yang GA, O.; Wenpei, W.; Sainan, Z. Physical model experimental study on deformation and failure of overlying rock slope under the condition of steep coal seam mining. *J. Geomech.* **2018**, *24*, 399–406.
33. Liu, C.; Xiao, R. Mechanism analysis on Yanchihe avalanche disaster in Yuan’an, Hubei. *J. Catastrophology* **2021**, *36*, 130–133, 150.
34. Lian, Z.P.; Tan, J.M.; Li, J.F. Stability evaluation of Yanchihe phosphate mine in Yuan’an, Yichang, China. *Geol. Miner. Resour. South China* **2013**, *29*, 60–65.
35. Yao, B.; Sun, Y. Rockfall and Its Failure Mechanism of Yanchihe Phosphate Mine in Yichang. *Typ. Landslides China* **1986**, *10*, 89–98.
36. Xu, Y.; Yin, Z.; Zhang, N.; Sa, L. Analysis of the cause of Toutun large scale landslide in Zhenxiong county, Yunnan province. *Chin. J. Geol. Hazard Control* **2015**, *26*, 6–11+24.
37. Yin, Y.; Liu, C.; Chen, H.; Ren, J.; Zhu, C. Investigation on catastrophic landslide of January 11, 2013 at Zhaojiagou, Zhenxiong county, yunnan province. *J. Geomech.* **2013**, *21*, 6–15.
38. Chen, G. Analysis on Collapse Disaster and Formation Mechanism of Furong Mountain. *J. Xi’an Min. Inst.* **1999**, *2*, 24–25+47.
39. Wang, Z.; Yan, E.; Yin, X.; Zhang, Q.; Tang, R. Study on collapse mechanism of anti-inclined rock slope: A case study of Honglianchi Iron Mine slope in Hefeng, Hubei. *J. Cent. South Univ. (Sci. Technol.)* **2014**, *45*, 2295–2302.
40. Huang, G. Research of the Mechanism of Deformation and Failure of Rock Slope above the Underground Goaf-Taking the Deformable Body of Yunlong Mountain in Dafang County of Guizhou Province as an Example. Ph.D. Thesis, Chengdu University of Technology, Chengdu, China, 2013.
41. Tuan, N.Q. Analysis of Rock Slope Failure and Rockfall for Preliminary Hazard Assessment of the Cliff at Chau Thoi Quarry. In Proceedings of the International Conference on Innovations for Sustainable and Responsible Mining; Springer: Berlin/Heidelberg, Germany, 2021; pp. 230–249.
42. Be, P.; Brouardb, B.; Feuga, B.; Karimi-Jafari, M. The 1873 collapse of the Saint-Maximilien panel at the Varangeville salt mine. *Int. J. Rock Mech. Min. Sci.* **2008**, *45*, 1025–1043.
43. Del Ventisette, C.; Gigli, G.; Bonini, M.; Corti, G.; Montanari, D.; Santoro, S.; Sani, F.; Fanti, R.; Casagli, N. Insights from analogue modelling into the deformation mechanism of the Vaiont landslide. *Geomorphology* **2015**, *228*, 52–59. [[CrossRef](#)]
44. Tokgoz, N. Case study of the Agacli landslide-gully complex during post-coal-mining reclamation and afforestation. *Environ. Earth Sci.* **2009**, *59*, 1559–1567. [[CrossRef](#)]
45. Mezam, M.C.; Assed, M.A.B. Retro-analytic study of the Northeastern edge landslide of Kef Essenoun open pit mine (Djebel Onk), Algeria. *Bull. Eng. Geol. Environ.* **2017**, *76*, 1307. [[CrossRef](#)]
46. Gage, H.J.; Eyles, C.H.; Peace, A.L. Winter weathering of fractured sedimentary rocks in a temperate climate: Observation of freeze–thaw and thermal processes on the Niagara Escarpment, Hamilton, Ontario. *Geol. Mag.* **2022**, 1–22. [[CrossRef](#)]

47. Yin, N.; Yu, Z.; Shi, Y.; Fu, G. New Active Characteristics and Seismological Significance of the Yuan'an Fault in the Central Hubei Basin. *J. Seismol. Res.* **2021**, *44*, 607–612.
48. Liu, H.; Zhang, B.; Li, Y.; Zhang, X. Stability Analysis and Formation Mechanisms of 'Yizhuxiang' Dangerous Rock Mass in Yanchi Village, Leizu Town, Yuanan County. *Resour. Environ. Eng.* **2017**, *31*, 574–580.
49. Ferrara, V.; Pappalardo, G. Kinematic analysis of rock falls in an urban area: The case of Castelmola hill near Taormina (Sicily, Italy). *Geomorphology* **2005**, *66*, 373–383. [[CrossRef](#)]
50. Li, B.; Wang, G.; Feng, Z.; Wang, W. Failure mechanism of steeply inclined rock slopes induced by underground mining. *Chin. J. Rock Mech. Eng.* **2015**, *34*, 1148–1161.
51. Zheng, D.; Li, K.; Wu, Y. Experimental study on influence of moisture content on shear property of dolomite. *Min. Res. Dev.* **2013**, *33*, 20–23, 51.
52. Dipova, N. Preliminary assessments on the modes of instability of the Antalya (SW-Turkey) coastal cliffs. *Environ. Earth Sci.* **2009**, *59*, 547–560. [[CrossRef](#)]
53. Graf, K.; Rathmayr, B.; Raemy, V. Rock Avalanche Investigation in Tempi Valley, Greece. *Eng. Geol. Soc. Territ.* **2015**, *2*, 2049–2052.
54. Zhou, C.; Huang, W.; Ai, D.; Xu, H.; Yuan, J.; Kou, L.; Luo, X. Catastrophic landslide triggered by extreme rainfall in Chongqing, China: July 13, 2020, Ni-uerwan landslide. *Landslides* **2022**, *19*, 2397–2407. [[CrossRef](#)]
55. Zhou, C.; Ai, D.; Huang, W.; Xu, H.; Ma, L.; Chen, L.; Wang, L. Emergency survey and stability analysis of a rainfall-induced soil-Rock mixture landslide at chongqing city, China. *Front. Earth Sci.* **2021**, *9*, 774200. [[CrossRef](#)]
56. Zou, X. Study on the Aging Characteristics of Freeze-Thaw in Alpine Clod Rock Slope. Ph.D. Thesis, Chengdu University of Technology, Chengdu, China, 2012.
57. Tan, H.; Li, B.; Li, J.; Yuan, W.; Li, Z. Stability analysis of dolomite slope with freeze-thaw cycles. *Sci. Technol. Eng.* **2020**, *20*, 13825–13832.
58. Li, J.; Yuan, W.; Wang, W.; Li, Z. Physical and Mechanical Properties of Dolomite with Freeze-thaw Cycles. *Sci. Technol. Eng.* **2020**, *20*, 755–762.
59. Park, K.; Kim, K.; Lee, K.; Kim, D. Analysis of Effects of Rock Physical Properties Changes from Freeze-Thaw Weathering in Ny-Ålesund Region: Part 1—Experimental Study. *Appl. Sci.* **2020**, *10*, 1707. [[CrossRef](#)]
60. Mu, J. The Rock Degradation Damage Characteristics and the Disaster-Causing Effects under the Cyclic Freeze—Thaw Action. Ph.D. Thesis, Chengdu University of Technology, Chengdu, China, 2013.
61. Liu, H.; Wang YWang, H.; Hou, Z. Experimental study on frost heaving pressure evolution of rock ice cracks under freezing-thawing cycles. *J. Eng. Geol.* **2022**, *30*, 1122–1131.
62. Nakamura, D.; Goto, T.; Suzuki, T.; Ito, Y. Basic Study on the frost heave pressure of rocks-dependence of the location of frost heave on the strength of the rock. *J. MMIJ* **2012**, 124–133.
63. Qiao, C.; Wang, Y.; Song, Z.; Li, C.; Hou, Z. Experimental study on the evolution characteristics of cyclic frost heaving pressure of saturated fractured granite. *Rock Soil Mech.* **2021**, *42*, 2141–2150.
64. Chen, Z.; Wang, L.; Wang, S.; Li, J.; Xu, Y.; Xiang, L. Loading and Unloading Mechanical Characteristics of rock under Freezing-thawing Cycles. *J. Yangtze River Sci. Res. Inst.* **2017**, *34*, 98–103.
65. Salmi, E.F.; Karakus, M.; Nazem, M. Assessing the effects of rock mass gradual deterioration on the long-term stability of abandoned mine workings and the mechanisms of post-mining subsidence—A case study of Castle Fields mine. *Tunn. Undergr. Space Technol.* **2019**, *88*, 169–185. [[CrossRef](#)]
66. Luo, R.; Li, G.; Chen, L.; Yang, Q.; Zang, C.; Cao, W. Ground subsidence induced by pillar deterioration in abandoned mine districts. *J. Cent. South Univ.* **2020**, *27*, 2160–2172. [[CrossRef](#)]
67. Zhou, Y.; He, Y. Pillar Stability Analysis in Common Room-and-pillar Mining Method. *Value Eng.* **2014**, *18*, 54–55.
68. Ali, H.; Kaveh, A.; Parviz, M.; Kamran, G. Numerical investigation of the impact of geological discontinuities on the propagation of ground vibrations. *Geomech. Eng.* **2018**, *14*, 545–552.
69. Zhou, C.; Ma, W.; Sui, W. Transparent soil model test of a landslide with umbrella-shaped anchors and different slope angles in response to rapid drawdown. *Eng. Geol.* **2022**, *307*, 1–14. [[CrossRef](#)]

Disclaimer/Publisher's Note: The statements, opinions and data contained in all publications are solely those of the individual author(s) and contributor(s) and not of MDPI and/or the editor(s). MDPI and/or the editor(s) disclaim responsibility for any injury to people or property resulting from any ideas, methods, instructions or products referred to in the content.